

ANTHROPOMORPHIC PHANTOMS FOR ASSESSING SYSTEMS USED IN
ULTRASOUND IMAGING OF THE COMPRESSED BREAST

by Ernest L. Madsen,* Elizabeth Kelly-Fry† and Gary R. Frank*

* Medical Physics Department
University of Wisconsin, Madison, WI 53706

† Indiana University School of Medicine and the Indianapolis Center for
Advanced Research, Indianapolis, IN

ABSTRACT -- Two anthropomorphic phantoms, simulating the breast as it is compressed against the chest wall during ultrasonic imaging, are described in detail regarding structural configurations and distributions of ultrasonic properties. The external shape of each phantom is that of a rectangular parallelepiped; this simple shape is consistent with the breast in the compressed configuration and also facilitates the inclusion of a considerable variety of simulated lesions including comparisons of imaging as a function of depth.

One of the phantoms was completed about 4 1/2 years prior to this writing, and images made with scanners which were state-of-the-art in late 1983 and 1984 are compared with images made with two current state-of-the-art imagers. Improvements in imager quality over that period are apparent.

The more recently produced phantom contains a simulated tumor with a complex structure as well as realistic simulated calcifications of various sizes. The tumor has a necrotic core and an irregularly shaped boundary. This boundary possesses a roughness intended to give rise to diffuse reflection.

Key words: phantom, model, simulation, breast, ultrasound, sonography, calcifications, anthropomorphic, lesions, tumor.

I. INTRODUCTION

To a large extent, present day clinical ultrasound pulse-echo imaging is performed with the breast compressed against the chest wall. A number of possible advantages are associated with this configuration (Kelly-Fry, 1985a). One is that use of higher frequency interrogating beams - with perhaps better resolution - is facilitated because of the reduced tissue depth and the consequent reduced net attenuation of the tissue lying between the scanning head and the tissue of concern. A second advantage is the tendency for image degrading at refraction interfaces - such as those between a fatty and nonfatty region - to be minimized due to the flattening of refracting interfaces.

Two anthropomorphic breast phantoms, constructed to simulate the breast in its compressed configuration, are reported. Each phantom contains successive layers of simulated skin, subcutaneous fat, glandular region, retromammary fat, and pectoral muscle. Simulated abnormal objects of various types are positioned in the glandular regions.

The two phantoms test ultrasound breast imagers in very different ways. This fact results from fundamental differences in their internal structures. All of the simulated abnormal objects in the larger of the two phantoms (phantom I) are spheres having diameters ranging from 3 mm to 19 mm. The smaller of the two phantoms (phantom II) has a few spherical objects, but

the most significant simulated abnormal objects are not spherical; e.g., a simulated malignant tumor has an irregularly shaped boundary and a central highly attenuating necrotic core. Also, there are regions containing simulated calcifications, most of which are polycrystalline calcium hydroxyapatite clumps. Other differences between the phantoms are: 25% of the volume of the glandular region of phantom I consists of tissue-mimicking (TM) fat spheres, and no such fat spheres are in phantom II; a significant property of phantom I, not existing in phantom II, is that rows of three identical simulated lesions are present, the differentiating parameter being their depth in the glandular region; lastly, the simulated pectoral muscle in phantom I contains closely packed simulated muscle bundles, and such muscle bundles are not present in phantom II.

The structure and ultrasonic properties of both phantoms are described in detail and images made with laboratory and clinical pulse-echo ultrasound scanners are presented and discussed. Intercomparisons can be made between scanners, based on their relative abilities to image various objects, and in some cases significant distinctions can be made. Regarding intercomparisons of scanners, images made with state-of-the-art scanners four years ago are compared with images made on the same phantom with two of today's state-of-the-art scanners; considerable improvement is demonstrated.

II. STRUCTURE AND BULK ULTRASONIC PROPERTIES

There are some differences in compositions of the various tissue-mimicking materials making up the two phantoms. Therefore, the two phantoms are described separately.

Methods for determining the ultrasonic properties of the component materials have been described in previous publications. All determinations were made at 22°C, a typical room temperature. Ultrasonic speeds and attenuation coefficients were determined using the water path displacement method (Madsen et al., 1978; Madsen et al., 1982a). Densities were determined through direct means (Madsen et al., 1982a). Absolute backscatter coefficients were determined for the materials in phantom II via a method described previously (Madsen et al., 1984). In phantom I only relative backscatter coefficients were determined by means of B-scan comparisons of mean texture grey levels using a scanner with a calibrated gain control. For the past 4 1/2 years phantom I has been extensively tested at the Indiana University Medical Center, particularly with respect to correlation of *in-vivo* breast images with phantom images. In addition, using a spectrum analyzer, techniques were developed for comparing the center frequencies and band widths of signals received from breast subcutaneous fat, parenchyma, and muscle with those received from the corresponding regions of the phantom (Kelly-Fry et al., 1987).

Phantom I

Diagrams of phantom I are shown in Figs. 1a, b, and c. The phantom has the outer shape of a rectangular parallelepiped, 24cmx10cmx5.5cm, with a 0.127 mm thick Teflon scanning window on one of the two largest sides. Fig. 1a shows a view of the phantom from scanning window side.

Six rows of three simulated lesions, each lesion identical to the other two, are shown. The rows are lettered A, B, C, E, F, and G. (Note that the missing letter D in this set of letters has been reserved for designating two unlike simulated masses described below.) The lesions in any one of these rows differ with respect to their depth in the glandular region. These depth differences are illustrated in Figs. 1b and 1c.

The simulated lesions in any one of the six rows differ in one or more ways from those in the other five rows. The spheres in row A are 6.3 mm diameter spheres of polyurethane exhibiting very high attenuation and no internal echo sources. The spheres in row G consist of the same polyurethane material, but the diameter is 3 mm instead of 6.3 mm. Rows B and F consist of spheres in which the attenuation coefficient at any frequency is nearly the same as that of their surroundings, while the backscatter coefficient is 6 dB below that of the surroundings; the spheres in row B are 6.3 mm in diameter and those in row F are 9.5 mm in diameter. The spheres in row C and E simulate cysts, attenuate less than the surroundings, and have negligible echogenicity; those in row C are 6.3 mm in diameter and those in row E are 9.5 mm in diameter.

The remaining two spheres near the center of the phantom are 12.7 mm in diameter. The row which they define is labeled D. That below the subareolar zone (Fig. 1c) consists of TM fat and the other simulates a cyst

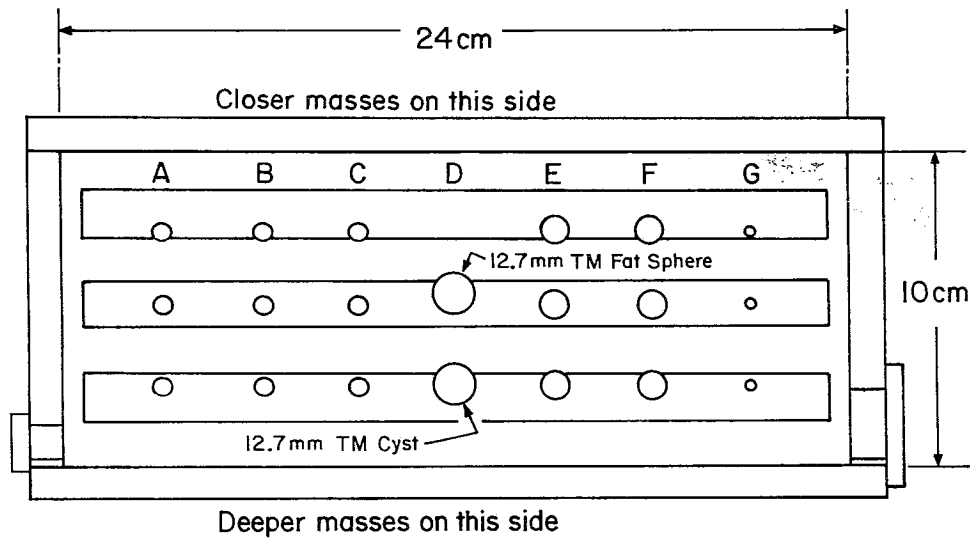


Fig. 1a. Diagram of phantom I viewed through the scanning window. Rows A, B, C, E, F and G each contain three identical spherical simulated lesions suspended in the tissue-mimicking (TM) glandular region. Row D contains two 12.7 mm diameter spherical objects, the upper one, a TM fat sphere and the lower one a TM cyst.

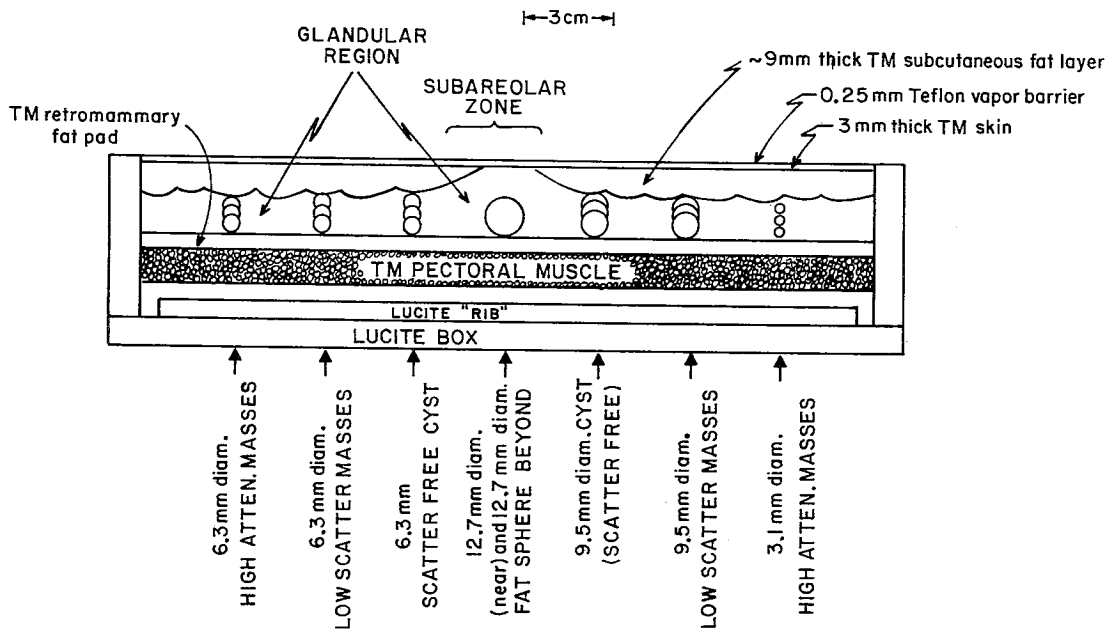


Fig. 1b. Side view diagram of phantom I showing the various layers of TM material and the different depths of the simulated lesions. An end view of the 1 mm diameter stacked agar grids simulating pectoral muscle bundles is shown. Also note the undulating interface between the TM subcutaneous fat layer and the glandular region.

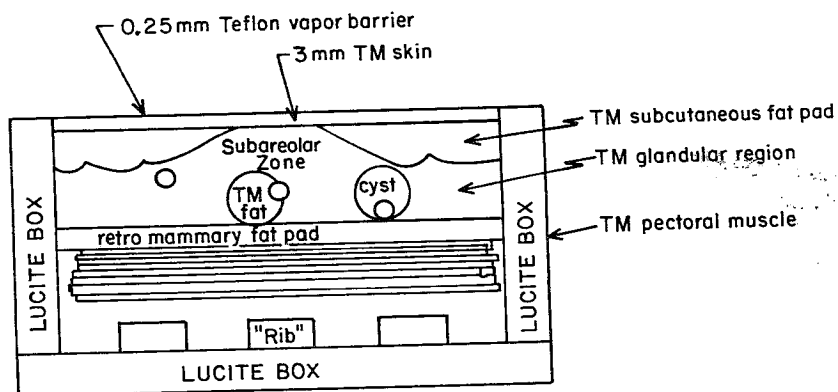


Fig. 1c. End view diagram of phantom I again showing the different depths of the lesions in the identical sets of three.

and is composed of the same material as that forming the spheres in rows C and E. The TM fat gives rise to a lower echogenicity than its surroundings.

The tissue-mimicking (TM) glandular region is formed from two components. Twenty-five percent of its volume consists of spheres of TM fat varying in diameter from 3 through 6 mm. The remaining seventy-five percent consists of TM nonfat.

The simulated normal tissues are designated in Fig 1c. A TM subcutaneous fat layer exists between the glandular region and the TM skin, and the TM skin is in contact with the 0.127 mm thick Teflon scanning window. A TM retromammary fat pad lies distal to the glandular region (distal with respect to the scanning window). Distal to the TM retromammary fat pad is the TM pectoral muscle, which consists of closely packed, parallel, 2 mm diameter agar rods surrounded with a much more dense and much more attenuating material. Finally, three parallel plexiglas "ribs" lie distal to the TM pectoral muscle.

In Table 1 are shown relevant values for ultrasonic speeds, slopes of the attenuation coefficients, and densities for phantom I.

Phantom II

The phantom and its contents are diagrammed in Figs. 2a and 2b. The external dimensions of the tissue-mimicking materials are 5.5cmx8cmx15cm. As in phantom I there are five contiguous layers, and these are shown in Fig. 2a. In order of increasing distance from the 0.127 mm thick Teflon scanning window, they are: a 3 mm thick layer of TM skin, a TM subcutaneous fat layer, TM glandular parenchyma, TM retromammary fat pad, and TM pectoral muscle. As mentioned above, there are no spheres of TM fat distributed in the layer of TM glandular parenchyma. Also, the TM pectoral muscle in phantom II does not contain simulated muscle bundles as in the case of phantom I. The TM muscle in phantom II is very similar to that composing the TM glandular parenchyma, although the slope of an attenuation coefficient is greater, as would likely be the case *in vivo*.

The simulated abnormal inclusions lie in the TM glandular parenchyma and these are best depicted in Fig. 2b. Two of these are homogeneous spherical simulated lesions. The upper lesion in the figure is a 12.7 mm diameter simulated TM cyst, and the lower is a 4 mm diameter simulated lower scatter lesion. To the right of the simulated cyst there is a relatively complex simulated tumor consisting of two parts, viz. a central 4 mm diameter, highly attenuating, simulated necrotic core, and a surrounding simulated vital tumor layer with an irregular boundary and a lower echogenicity compared to that of the surrounding TM glandular parenchyma; the irregular boundary also has a "rough" surface corresponding to irregular undulations having a spacing and depth range of about 1/2 mm. The mean diameter of this tumor is about 15 mm. To the right of this simulated

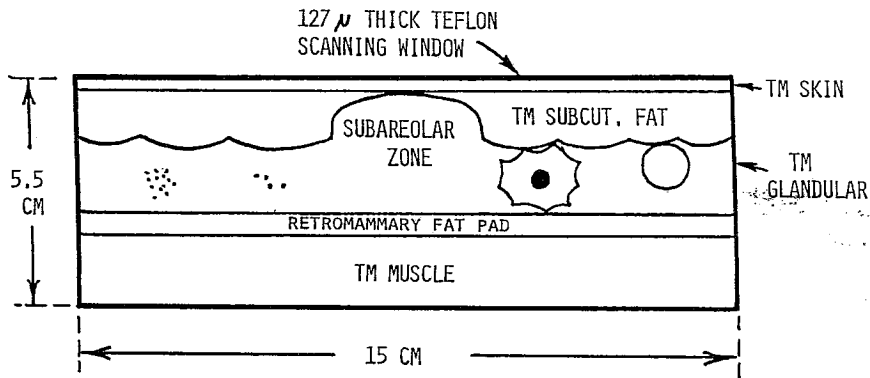


Fig. 2a. Side view diagram of the contents of phantom I including calcifications and a simulated malignancy with a necrotic core. The 8cmx15cm scanning window is perpendicular to the figure.

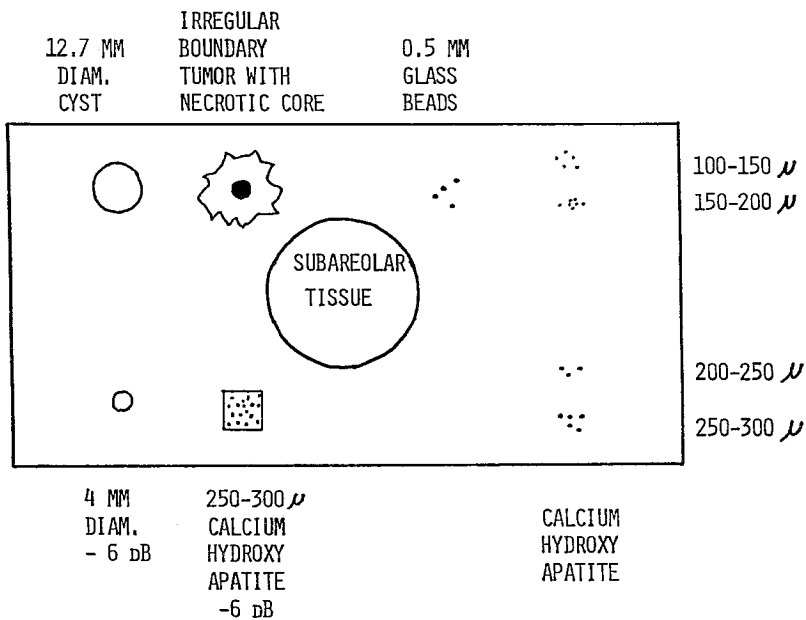


Fig. 2b. Diagrammatic view of anthropomorphic compressed breast phantom II from the scanning window side. Various objects are imbedded in the TM glandular parenchyma. Six sets of simulated calcification are shown, five of which are Calcium hydroxyapatite, which is the inorganic component of bone. The leftmost set of calcifications are randomly suspended in a 0.5 cm³ volume of TM abnormal tissue having a - 6 dB scatter level relative to the TM glandular parenchyma. Also shown is a realistic simulated tumor with an irregular boundary and a highly attenuating necrotic core. The vital part of the tumor is at - 6 dB scatter level relative to the glandular parenchyma except for two small "chips" of higher scatter material present to produce an irregular internal texture.

Table 1. Ultrasonic properties of component tissue-mimicking (TM) materials in phantom I at 22°C. Relative backscatter levels are discussed in the text.

TM material	Ultrasonic speed (m/s)	Slope of the attenuation coefficient (dB/cm/MHz)	Density (g/cm ³)
Subcutaneous fat	1456	0.47	0.94
Retromammary fat and 12.7 mm diam. fat sphere	1458	0.54	0.94
Glandular parenchyma	1569	0.34	1.03
Fat spheres composing 25% of glandular region	1445	0.3	0.92
Cysts	1568	0.1	1.02
Low scatter lesions ("fibroadenomas")	1564	0.34	1.03
High attenuation lesions	1508	8.7 at 3 MHz	1.05
Pectoral muscle	1540	0.4	1.08
Skin	1570	0.6	1.05

complex tumor is a set of four 0.5 mm diameter spherical glass beads to simulate calcifications. These are a few mm from one another and are embedded in the TM glandular parenchyma. Opposite the irregularly bounded simulated tumor is a cube (~ 8 mm side) of TM nonfat material having the same attenuation coefficient as that of the TM glandular parenchyma and a backscatter coefficient 6 dB below that of the TM glandular parenchyma; randomly distributed in this cube are about twenty polycrystalline chunks, or particles, of calcium hydroxyapatite with diameters ranging from 250 μm to 300 μm . Four other clusters of polycrystalline calcium hydroxyapatite particles are shown on the right side in Fig. 2b. Each particle approximates a sphere and each cluster contains three to five particles, the mean diameter distinguishing the four clusters from one another. The four diameter ranges are 100-150 μm , 150-200 μm , 200-250 μm , and 250-300 μm . Note that the latter diameter range is the same as that of the particles in the cube with a reduced backscatter coefficient. All four of the clusters on the right are imbedded in the TM glandular parenchyma itself.

In Table 2 are shown relevant ultrasonic properties of the component materials in phantom II.

Table 2. Ultrasonic properties of TM materials in phantom II at 22°C:
 c = ultrasonic speed; α/f = slope of the attenuation coefficient with frequency; ρ = density; η = backscatter coefficient.

TM material	c (m/s)	α/f (dB/cm/MHz)	ρ gm/ml	η ($\text{sr}^{-1}\text{cm}^{-1}$)	η at 5 MHz relative to glandular (dB)
TM glandular	1561	0.36	1.04	4.4×10^{-3} *	0
Subcutaneous fat	1458	0.43	0.94		-12
Retro-mammary fat	1458	0.40	0.94		-11
Tumor around necrotic core	1554	0.70	1.07		-6
Low scatter lesion with calcifications	1556	0.56	1.06		-6
Muscle	1559	0.55	1.05		+6
low scatter 4 mm mass	1561	0.33	1.04		-6
cyst	1560	0.12	1.02		--

* *in vivo* breast glandular tissue at 5 MHz: $\eta \sim 6 \times 10^{-3} \text{ sr}^{-1}\text{cm}^{-1}$ (Davros et al., 1986)

III. MATERIALS

Except for the TM fat spheres suspended in the glandular parenchyma of phantom I and agar rods in the TM pectoral muscle of that phantom, all tissue-mimicking materials in the phantoms consist of a water-based gelatin (derived from calf skin) containing suspended microscopic particles (Madsen et al., 1978; Madsen, 1980). Five percent of the liquid component consists of n-propanol. There also is a small concentration ($\sim 0.2\%$) of formaldehyde which, through cross-linking of the gelatin molecules, produces thermal stability by raising the melting point of the materials to over 100°C (Madsen, 1980).

In the case of the TM subcutaneous fat layer and retromammary fat pad, the suspended particles consist of oil; the oil is a solution of half olive oil and half kerosene. The volume fraction of the TM fat consisting of oil is 50%. (The 3 mm through 6 mm diameter TM fat spheres, composing 25% of the volume of the glandular region in phantom I, consist of nearly the same material as that composing the above layers, the exception being that agar gel replaces the animal hide gel as the non-oil component.) The TM fat materials and their method of production are described in detail in a previous publication (Madsen et al., 1982a).

The particles in the TM nonfat materials are solid and are less than 100 μm in diameter. Only about 2 or 3 percent of the volumes of these materials consists of particles. The larger particles give rise to any significant ultrasonic scattering produced and the smaller (ranging down to as small as 1 μm in diameter) give rise mainly to absorption (Wu et al. 1988). The particles giving rise to both absorption and scattering in the TM skin of phantom I are talc. The talc tends to yield a higher ratio for backscatter coefficient to attenuation coefficient than the graphite in phantom I. This higher ratio is the reason talc was used in making the TM skin. At the time of construction of phantom I, independent control of absorption and scattering via finely powdered graphite and larger glass beads, respectively, had not yet been instituted in our lab.

As just mentioned, the background echo patterns in the TM nonfat materials of both phantoms involves scattering by spatially random distributions of particles somewhat less than 100 μm in diameter. In the case of phantom I - with the exception of the TM skin - all solid particles in these materials are graphite and their diameter range extends from about 1 μm through 100 μm . These graphite particles are responsible for both the scattering and absorptive components of the attenuation coefficients.

In phantom II, the background echo patterns in the TM nonfat materials occur as a result of scattering by a spatially random distribution of glass beads, 75 μm to 90 μm in diameter. The absorptive component of the attenuation results almost entirely from the presence of the remaining solid particles. The latter consist of graphite and have diameters less than 22 μm . These graphite particles contribute negligibly to scattering. Thus, for the TM nonfat materials used in phantom II, independent control of the scattering and absorptive components existed.

The TM pectoral muscle of phantom I also differs from that of phantom II. That in phantom I being more complex and a better representation of muscle. The TM pectoral muscle in phantom II is a version of the TM nonfat containing a spatially random distribution of glass 75 to 90 μm glass beads and graphite powder with diameters less than 22 μm .

The TM pectoral muscle in phantom I consists of closely packed, parallel agar rods, the interstices between these rods being filled with animal hide gelatin with a relatively high concentration of 1-100 μm diameter graphite particles. The rods are stacked parallel to the 10 cm long side of the rectangular scanning window. Each rod is about 9.5 cm long and is 2 mm in diameter. The 2 mm diameter is representative of the diameter of muscle bundles in real muscle. Significant differences in both density and ultrasonic speed exist between the agar rod material and the material in the interstices. These differences mean that ultrasonic scattering related to the boundaries between muscle bundles is simulated. Except for the fact that agar rods are used instead of agar spheres, this TM pectoral muscle is identical in composition to "TM liver B" described in detail in a previous publication (Madsen et al., 1982b).

To mimic highly attenuating tumor tissue in both phantoms, spheres of polyurethane were cast using a two part resin (Devcon Flexane, Devcon Corp., Danvers, Massachusetts). No scatterers were embedded in the polyurethane.

Phantom II contains clusters of objects intended to mimic calcifications in the breast. The composition of the largest of these objects (0.5 mm diameter) is glass; the remainder are composed of calcium hydroxyapatite. The latter material could be the dominant component of calcifications associated with breast malignancies (Frappart et al., 1984 and 1986).

IV. IMAGES OF THE PHANTOMS

Since there are a considerable number of objects to be imaged in the phantoms, it is necessary to minimize the number of imaging examples while still illustrating the realism and usefulness of the phantoms.

Phantom I

Many of the images of phantom I were made using scanners which were state-of-the-art four years prior to this writing. These images are shown along with images made on a present day (1987-1988) state-of-the-art scanner suitable for breast imaging. The images in Figs. 3 - 9 were made in late 1983 and 1984 using the older scanners and images in Figs. 10 - 18 were made with present-day state-of-the-art scanners.

In Fig. 3 is shown an image made with a modified Life Instruments automated waterpath scanner which was undergoing clinical trials at the

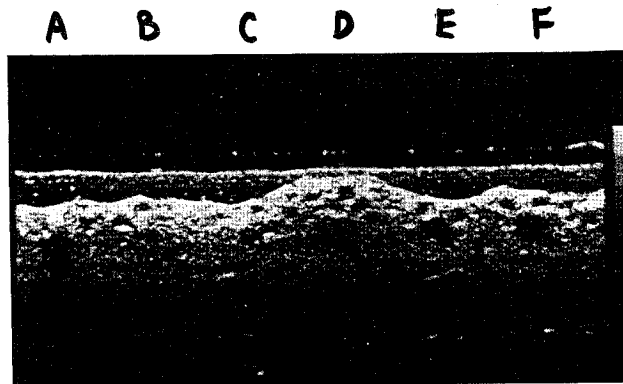


Fig. 3. Image slice along the long dimension of phantom I through the intermedicate depth lesions (excluding the 3 mm diameter high attenuation lesion which would be just off the right of the image). The scanner was made by Life Instruments. Identification of the various objects imaged can be inferred from Figs. 1b and 1c.

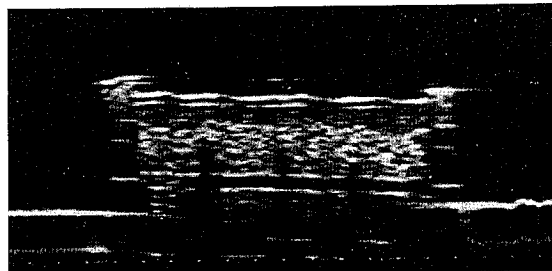


Fig. 4. Image slice through the 6.3 mm diameter high attenuation TM lesions of phantom I using a Technicare dedicated breast scanner operating at 3 MHz. Strong shadowing identifies all three lesions.

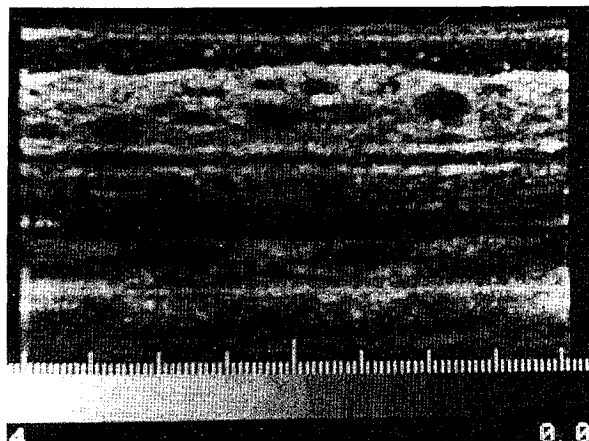


Fig. 5. Image of the three 9.5 mm diameter low scatter masses in phantom I made with a 4 MHz laboratory scanner at the Ontario Cancer Institute. Grey levels within the TM lesions are not well defined.

University of Toronto's Women's College Hospital at the time this scan was made. The 4 MHz transducer assembly consisted of an annular array transmitter and conical PVDF receiver. The scanning plane is along the long dimension of the phantom and, referring to the diagrams in Figs. 1a and 1b, includes the central plane from the intermediate depth 6.3 mm diameter high attenuation mass on the left through the intermediate depth 9.5 mm diameter low scatter mass on the right. The subcutaneous fat layer is well differentiated from the glandular region, and the undulating interface between these two zones is well defined. TM fat spheres in the proximal part of the glandular region are also well defined. The strongly shadowing 6.3 mm diameter high attenuating mass is seen on the left side of the image (directly below the letter A). The 6.3 mm diameter TM low scatter mass (B) and 6.3 mm diameter TM cyst (C) are rather poorly defined; this poor definition may, however, be related to the fact that all imaged masses do not have their centers precisely coplanar. The 12.7 mm diameter TM fat sphere (D) is centrally located below the subareolar region. To the right of the latter is the image of the 9.5 mm diameter TM cyst (E). Lastly, the 9.5 mm diameter TM low scatter mass is the right-most imaged object (F). The quality of the image suffers considerably with increasing depth into the phantom. For example, the retromammary fat pad is only vaguely defined.

In Fig. 4 is shown an image also made in late 1983 with a Technicare automated waterpath breast scanner using a single focus transducer operating at 3.5 MHz. The scanning plane is perpendicular to the phantom diagram in Fig. 1b and passes through the centers of the three 6.3 mm high attenuation masses. All three masses were well defined in terms of strong shadowing and absence of echoes from within the masses. These three masses were easily imaged by all scanners employed in the late 1983 period. Notice, however, that resolution in Fig. 4 is not adequate for defining the TM fat spheres in the glandular parenchyma.

In Fig. 5 is shown an image of the 9.5 mm diameter low scatter masses made in late 1983 with a 4 MHz laboratory scanner at the Ontario Cancer Institute. The transducer assembly was of the same type as that employed in generating Fig. 3. All three masses are clearly defined as is the TM retromammary fat pad. The spherical masses are imaged in the form of ellipses because the instrumental vertical and horizontal scale factors had not yet been made equal in this laboratory system.

In Fig. 6 is shown an image of the 6.3 mm diameter low scatter masses made during the same period with the 4 MHz automated laboratory scanner at the Ontario Cancer Institute. The masses are below the x's in the figure. The deepest mass corresponds to the left-most x, and it is not imaged adequately for it to be detected without a priori knowledge. The other two are detected but are not well differentiated from the surrounding fat spheres. Notice that there is little evidence of echo "texture" within the two defined masses.

In Figs. 7a and 7b is shown an image, made in late 1983 using a clinical scanner at the Indiana University Medical Center, of the 6.3 mm diameter low scatter masses. In Fig. 7a these simulated masses are pointed out via three small + signs immediately to their right. In Fig. 7b the + signs are not present, allowing the reader to better judge the detectability of the masses. This automated breast scanner, developed by the Indianapolis Center for Advanced Research (ICFAR), featured a sharply focused 3.7 MHz transducer and water bag coupling. A modified version of this unit was subsequently marketed by Labsonics, Inc. The grey level echo texture in the proximal mass is well defined, but is not well defined in the intermediate and deeper masses. A possible reason for the lack of textural definition in the deeper two masses is the lack of time gain compensation in this early system.

In Fig. 8 is shown an image through the same three low scatter masses made with the Ausonics System 1 automated sector scanner operating with multiple single focus transducers at 4.5 MHz and using waterbath coupling. The excellent resolution of this system is apparent, but the grey level echo texture for the low scatter masses is not adequate.

The 3 mm diameter TM high attenuation masses forming row G (See Fig. 1a.) are composed of the same material constituting the 6.3 mm diameter ones. The two deeper 3 mm masses were difficult to image (four years ago), however, with any scanner. A priori knowledge of "where to look" was generally required for detectability. However, the most proximal 3 mm attenuating mass could generally be identified on the basis of shadowing. In Fig. 9 is shown an image, obtained in 1984 by scanning along the long dimension of the phantom with the ICFAR breast unit equipped with an F/3, 7.5 MHz polymer (PVDF) transducer (Kelly-Fry et al., 1984). The TM

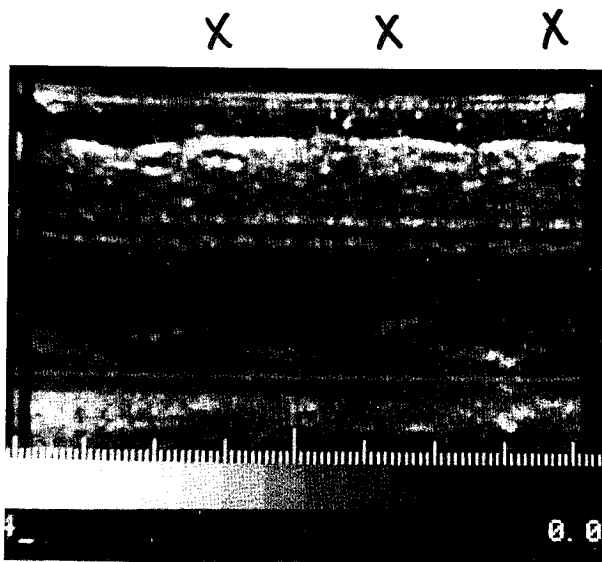
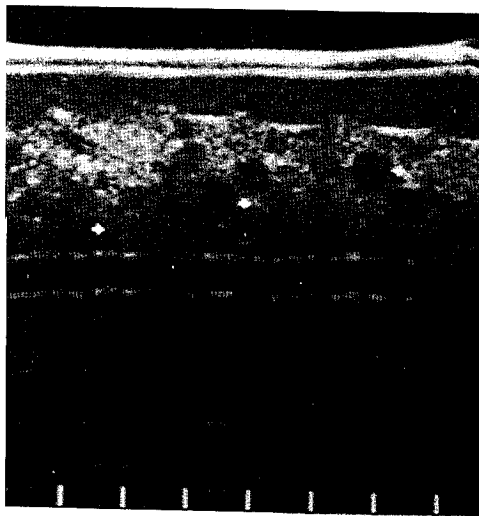
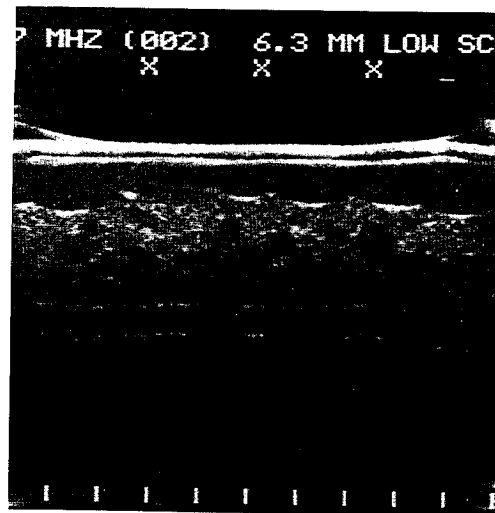


Fig. 6. Image of a slice of phantom I containing the three 6.3 mm diameter low scatter lesions. The scanner used was the 4 MHz laboratory scanner at the Ontario Cancer Institute. The x's lie on vertical lines passing through the three lesions. The proximal lesion is on the right. The intermediate depth lesion is obscured somewhat by the presence of a larger fat sphere to its upper right. The distal lesion has not been defined.



a



b

Fig. 7. Image slice of phantom I including the 6.3 mm diameter low scatter masses. The image was made using a 3.7 MHz ICFAR instrument. In 7a the image is shown with three + signs displayed just to the right of the three masses, and, in 7b, these + signs are absent allowing objective appraisal by the reader. (Note x's above each mass in 7b, but above the image.) The proximal lesion on the right is well defined including the reduced grey level texture pattern within it. The intermediate and distal lesions are less well defined.

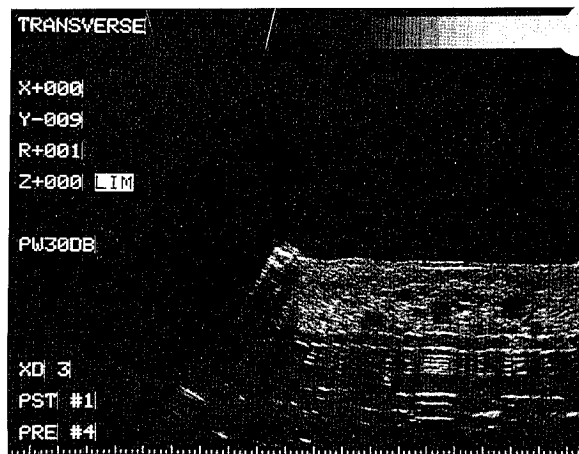


Fig. 8. Image slice of phantom I containing the three, 6.3 mm diameter low scatter lesions obtained with an Ausonics automated sector breast scanner operating at a frequency of 4.5 MHz. The image exhibits good resolution but grey levels within the 6.3 mm lesions are not well defined.

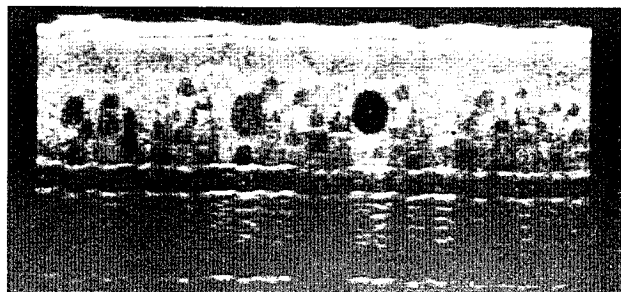
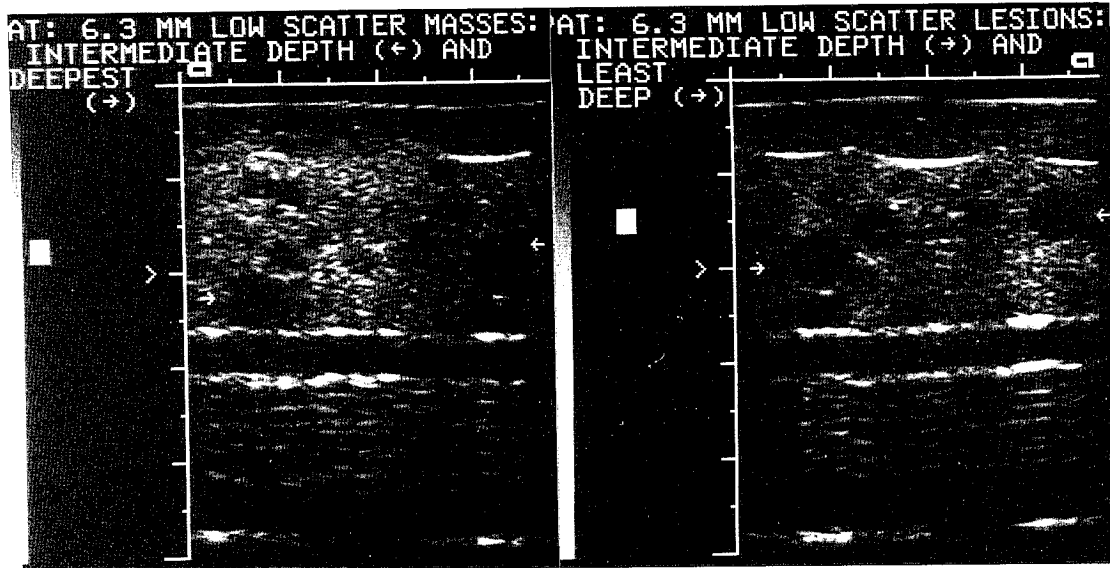


Fig. 9. Image of Phantom I obtained in 1984 by scanning along the long dimension of the phantom with a later version of the ICFAR breast unit than that used in generating Fig. 7. An F/3, 7.5 MHz polymer (PVDF) transducer was used.

subcutaneous fat layer, retromammary fat pad, and muscle bundles are well defined in this image. Note the precise characterization of the internal structure of the 9.5 mm low scatter mass, the sharp resolution of wall structures, and the distinctive imaging of the randomly positioned fat globules. [After further improvements in the sensitivity of the PVDF transducers, all three 3 mm attenuating masses were successfully imaged (Kelly-Fry, 1985b).]

In Figs. 10a, 10b and 11 are shown images made using an Acuson with the 3.8 cm long L538 5 MHz linear array. The scanning head was in direct contact with the phantom. This is the scanner currently used in breast imaging at the University of Wisconsin Hospitals. Advances in imaging quality can be observed by comparing these images with those obtained four years earlier.

In Fig. 10a and 10b is a pair of images showing the 6.3 mm diameter low scatter masses. Since the array transducer provides a linear scan that does not quite cover 4 cm, only two adjacent masses can be included in a single image. In Fig. 10b the proximal mass is imaged on the right (-) and the intermediate depth mass on the left (+). Notice the well defined echo texture levels within the masses. Other features are also well defined,



a

b

Fig. 10a. Image of the intermediate depth (-) and deepest (+) 6.3 mm diameter TM low scatter lesions in phantom I made recently using an Acuson imager with an L538 linear array. Grey level texture is displayed even within the deepest lesion.

Fig. 10b. Image of the proximal (-) and intermediate depth (+) 6.3 mm diameter TM low scatter lesions in phantom I made recently using the Acuson imager with an L538 linear array scanning head. Notice the well defined grey level texture within each lesion.

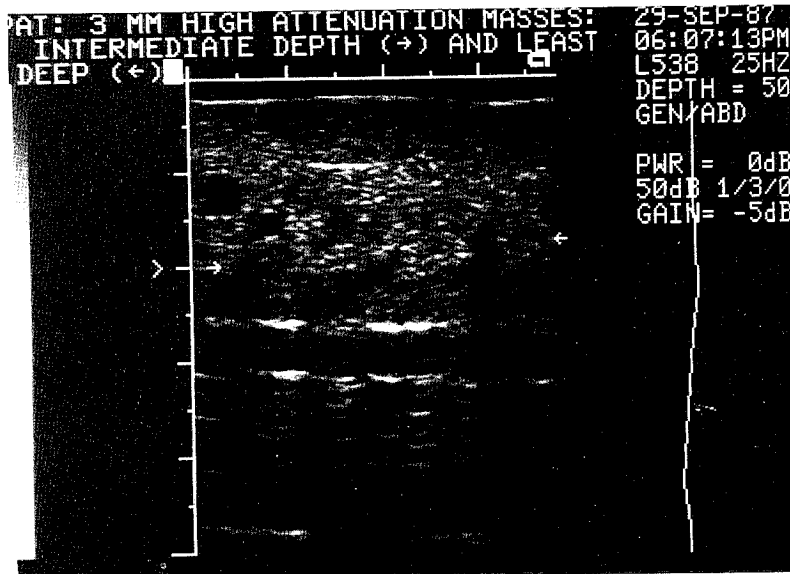


Fig. 11. Image of two of the 3 mm high attenuation lesions in phantom I made with the Acuson and L538 scanning head. The intermediate depth lesion is on the right (-) and the deepest is on the left (+).

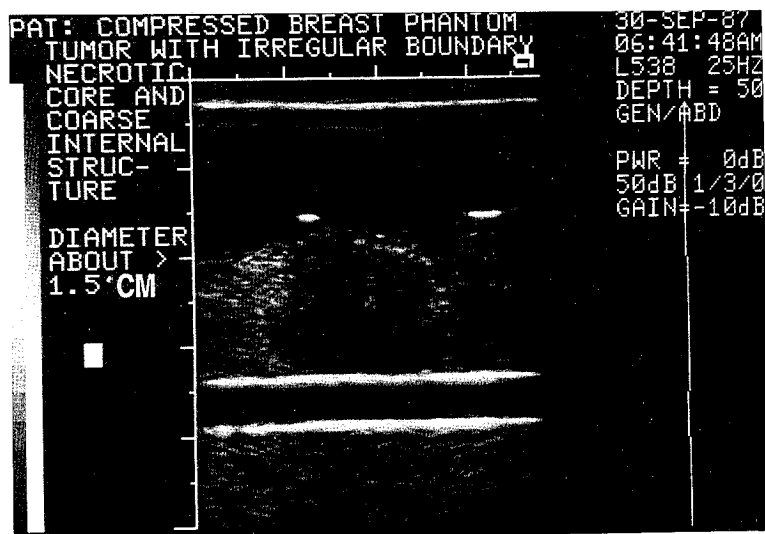


Fig. 12. Image using the Acuson and L538 scanning head of the simulated structurally complex tumor of phantom II; the image slice does not pass through the necrotic core.

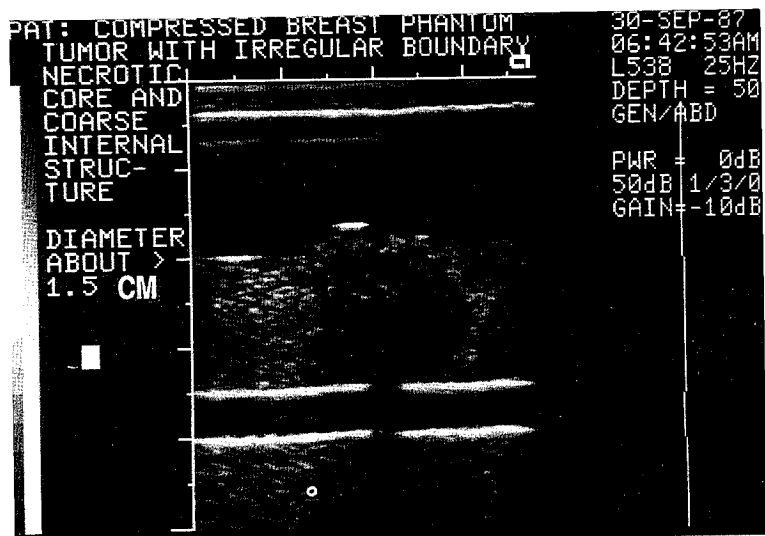


Fig. 13. Image using the Acuson and L538 scanning head of the simulated structurally complex tumor of phantom II; in this case the image slice does pass through the necrotic core.

e.g., the retromammary fat pad, the muscle bundles in the TM pectoral muscle, and the TM fat spheres in the glandular parenchyma. A large TM fat sphere with an accompanying specular reflection at its proximal surface is seen distal to the intermediate depth TM mass. In Fig. 10a the intermediate depth mass is on the right (-) and the deepest one on the left (-). The grey-level textural definition is very good even in the case of the deep mass. This grey level differentiation of scattering regions is far better than that in the images made four years ago.

In Fig. 11 is shown an image of two of the 3 mm diameter highly attenuating TM masses. That at the intermediate depth is on the right (-), and that at the greatest depth (in the glandular parenchyma) is on the left (-). The one at intermediate depth is well defined in terms of the considerable shadowing, while the deeper mass is only vaguely defined. The deeper mass lies just beneath two of the larger TM fat spheres and the related refraction effects have caused its obfuscation. The proximal 3 mm diameter high attenuation TM mass was very well defined.

Phantom II

All images of phantom II presented were made using one of two contemporary state-of-the-art scanning systems, viz, the Acuson with the 5 MHz L538 real-time scanning head and a high frequency (11 MHz), automated, tunable receiver scanner in current use at the Indiana University Medical Center (Kelly-Fry et al., 1988). These images are shown in Figs. 12 - 18. The images were made after September, 1987 since the manufacture of phantom II was not completed until then.

Recall that there are two distinguishing features of this phantom. One feature is a realistic simulated malignant tumor with a spiculated diffusely reflecting boundary and containing within it irregular scattering regions and a highly attenuating simulated necrotic core. The other feature is a

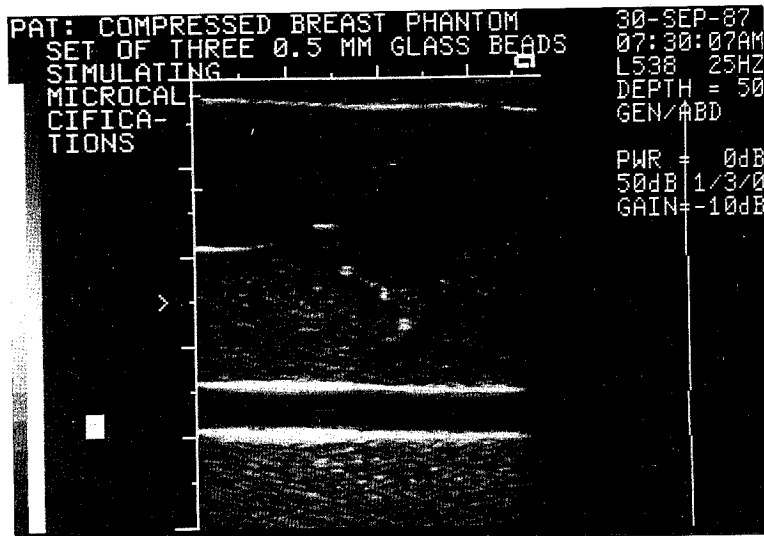


Fig. 14. Image of three of the 0.5 mm diameter spherical glass beads simulating calcifications in phantom II. The Acuson and L538 scanning head were used.

set of simulated calcifications, the emphasis again being on simulating the clinical situation as closely as possible. In Fig. 12 the scanning plane passes to one side of the simulated necrotic core. The lower scattering level within the bulk of the tumor is demonstrated (except for a higher scatter inhomogeneity near the center), and an irregularly shaped "halo" of elevated echo levels surrounds the tumor. The halo is presumably due to the roughened surface of the tumor, which was intentionally formed via the molding process.

In Fig. 13 is shown an image with the scanning plane passing through the highly attenuating necrotic core of the simulated tumor. A well defined shadow identifies the necrotic core.

In Fig. 14 is shown an image of three 0.5 mm glass beads suspended in the TM glandular parenchyma. The beads are clearly defined.

In Fig. 15 is shown an image for which the scanning plane passes through the 0.5 cm³ volume in which the mean backscatter level is 6 dB below that of the surrounding TM glandular parenchyma and in which there are randomly positioned about twenty 250 to 300 μ m diameter pieces of calcium hydroxyapatite. The arrow (->) points to an isolated echo which probably

corresponds to one of these pieces. Considerable scanning effort was expended to find evidence for the presence of these simulated calcifications, however, and no other calcium hydroxyapatite simulated calcifications were detectable.

For comparison purposes, Figs. 16 - 18 show images of phantom II obtained with the high frequency (11 MHz) tunable receiver breast scanner in operation at the Indiana University Medical Center (Kelly-Fry et al., 1988). The scanning plane in Fig. 16 is along the long dimension of the phantom; the 12.7 mm diameter cyst, the simulated malignant mass, and the 0.5 mm diameter glass beads have been imaged. The lower scattering level within the solid mass - and distinctive wall structure - are definitively imaged. The image shown in Fig. 17 was obtained along the same general scanning plane, except that the regions containing the 100-150 μm and 150-200 μm calcium hydroxyapatite particles are included. Note that the 100-150 μm and 150-200 μm calcium hydroxyapatite particles have not been detected. In Fig. 18 is shown an image through the 8x8x8 mm³ region containing approximately twenty 250-300 μm calcium hydroxyapatite particles and through the 4 mm diameter spherical mass. Recall that both the background of the 8x8x8 mm³ region and of the 4 mm mass have backscatter coefficients 6 dB below that of the surrounding glandular parenchyma. No evidence for the presence of the calcium hydroxyapatite particles is apparent, but the 4 mm diameter mass is clearly imaged.

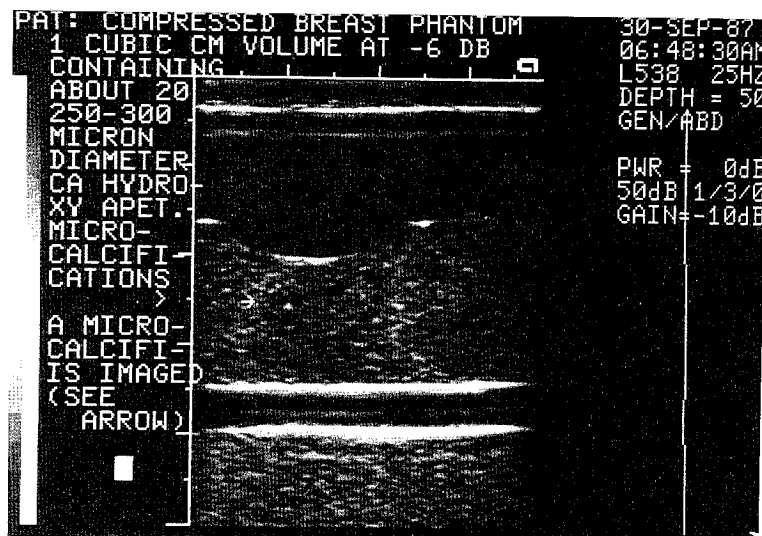


Fig. 15. Image of one of the 250-300 μm diameter calcium hydroxyapatite particles simulating calcifications in phantom II. The particle is imbedded in a 0.5 cm³ volume having a backscatter level 6 dB below that of the surrounding TM glandular parenchyma. The Acuson and L538 scanning head were used.

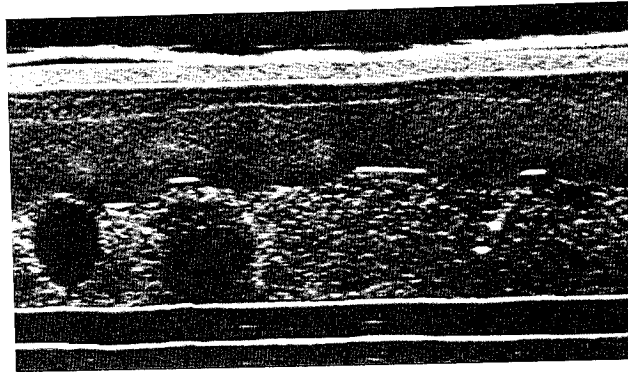


Fig. 16. Image of phantom II obtained by scanning along the long dimension of the phantom in the region of the cyst, simulated complex tumor and 0.5 mm beads. The image slice is through the simulated malignant mass. A high frequency (11 MHz) tunable receiver scanner, in use at Indianan University Medical Center, was used for these scans. MAG. 1.4:1

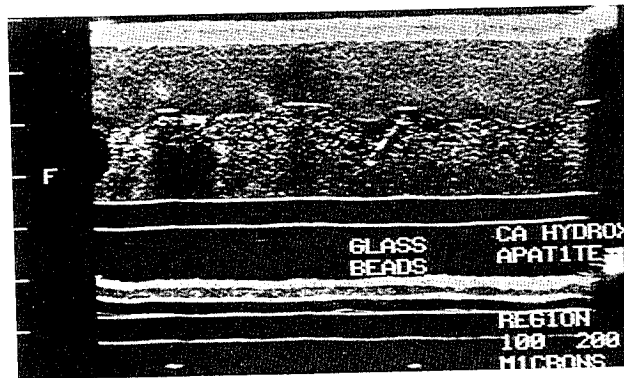


Fig. 17. Image of phantom II obtained by scanning along the same image plane of Fig. 16 except that the region containing the 100-200 μ m diameter calcium hydroxyapatite particles was included. A high frequency (11 MHz), tunable receiver scanner in use at Indiana University Medical Center was used for these scans.

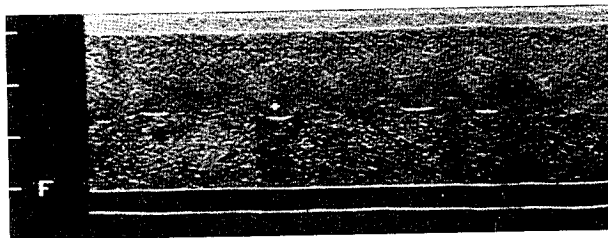


Fig. 18. Image of phantom II in region of: 1) 4mm spherical mass with a backscatter coefficient 6dB below the surrounding TM glandular parenchyma and 2) the 250-300 μ m hydroxyapatite particles suspended in an 8x8x8 mm³ volume (asterisk) at a backscattering level 6 dB below that of the surrounding TM glandular parenchyma. A high frequency (11 MHz) tunable receiver system in use at Indiana University Medical Center was used for these scans.

V. SUMMARY AND CONCLUSIONS

Two ultrasound anthropomorphic phantoms, corresponding to the breast as it is compressed against the chest wall during ultrasound imaging, have been described in detail regarding their material ultrasonic properties and regarding their internal and external configurations. Internally, the phantoms are composed entirely of ultrasonically tissue-mimicking materials.

One phantom (phantom I) was produced about 4 1/2 years before this writing and appears to have remained essentially unchanged during that time. Images of this phantom made with state-of-the-art ultrasound imagers four years ago are compared with those made with two present-day state-of-the-art imagers; all imagers were, or are, used for breast imaging. Considerable improvement in state-of-art ultrasound breast imaging over that period can be inferred. This improvement may warrant questioning current applicability of some negative assessments of ultrasound breast imaging, based on imaging with the older scanners (Kopans et al., 1985; Sickles et al., 1983; Sickles, 1985; Weber et al., 1985).

A major feature of phantom I is the assessment of imaging capability as a function of depth of the target in the TM glandular parenchyma. Inclusion of randomly positioned TM fat spheres throughout the glandular parenchyma challenges the imagers in terms of beam distortions due to refraction. The probability of serious impedance to imaging quality increases with increased depth of the imaging target, of course.

Phantom II was manufactured recently. A realistic representation of a malignant tumor is present; this realism is demonstrated in terms of the ultrasound images presented. Of particular significance is a halo-like echogenic boundary likely related to diffuse reflection at the roughened boundary of the tumor.

Also of considerable importance in phantom II is the inclusion of simulated calcifications. All such inclusions are embedded in material having a backscatter coefficient which is representative of breast tissue. If glass is a reasonable material for mimicking calcifications, then the phantom shows that 0.5 mm diameter calcifications can be easily detected. Representation of calcifications with glass beads has been done also in other laboratories (Kasumi, 1988). On the other hand, only one of about twenty 250 to 300 μ m diameter particles of calcium hydroxyapatite was detected in the phantom even though these particles were surrounded by material with a backscatter coefficient which is 6 dB below that of the TM glandular parenchyma. Other equal sized and smaller calcium hydroxyapatite particles were suspended in the TM glandular parenchyma, and determined attempts to detect them failed.

An important observation is that two contemporary state-of-the-art ultrasound instruments used in breast imaging cannot be expected to detect 300 μ m diameter calcifications which are embedded in glandular parenchyma. This observation includes the reasonable assumption that calcifications in vivo are similar in ultrasonic properties to calcium hydroxyapatite. An important aspect of a future phantom will be the inclusion of clusters of calcium hydroxyapatite particles with diameters greater than 300 μ m suspended in the TM glandular parenchyma; inclusion of comparably sized glass beads would also allow assessment of the appropriateness of glass beads for representing calcifications.

However, as indicated by Kasumi, calcifications can be ultrasonically detected in vivo if they are located within low echoic areas of malignant masses (Kasumi, 1983; Kasumi, 1988). It would be of interest, therefore, to include in the next breast phantom a set of submillimeter calcium hydroxyapatite particles within a low echoic region which is typical of malignant breast masses; this will require a study to estimate typical backscatter coefficients within malignant masses.

ACKNOWLEDGEMENTS

The authors are grateful to various people who arranged for ultrasound scans of phantom I. These include Profs. J.W. Hunt and F.S. Foster of the Ontario Cancer Institute. Also, the calcium hydroxyapatite particles were obtained from S. Bly while he was at the Ontario Cancer Institute, and we express our thanks to him.

This work was supported in part by NIH grant R01 CA25634.

REFERENCES

- Davros W.J., Zagzebski J.A. and Madsen E.L. (1986) Frequency-dependent angular scattering of ultrasound by tissue-mimicking materials and excised tissue. *J. Acoust. Soc. Am.* 80, 229-237.
- Frappart L., Boudeulle M., Boumendil J., Hu Chi Lin, Martinon I., Palayer C., Mallet-Guy Y., Raudrant D., Bremond A. and Rochet Y. (1984) Structure and composition of microcalcifications in benign and malignant lesions of the breast. *Hum. Pathol.* 16, 880-885.
- Frappart L., Remy I., Hu Chi Lin, Bremond A., Raudrant D., Grousseau B. and Vauzelle J.L. (1986) Different types of microcalcifications observed in breast pathology: correlations with histopathological diagnosis and radiological examination of operative specimens. *Virchows Arch. A.* 410, 179-187.
- Kasumi F. (1983) Ultrasound of the breast lesions. (In Japanese) Shinohara Publishing Co. pp. 138-156.
- Kasumi F. (1988) Can microcalcifications located within breast carcinomas be detected by ultrasound imaging? (Paper in this publication).
- Kelly-Fry E., Jackson V., Madsen E.L., Zagzebski J.A. (Sept. 1984) Use of 7.5MHz PVDF transducers to examine solid breast masses in the *in vivo* compressed breast and in a compressed breast phantom. *Proc. Am. Inst. of Ultra. in Med.*, Kansas City, MO
- Kelly-Fry E. (1985a) Influences on the development in the United States of ultrasound pulse-echo breast instrumentation. *In: Ultrasound Mammography*, Harper AP ed. University Press, Baltimore, Maryland.
- Kelly-Fry E. (1985b) Improving ultrasound mammography instrumentation; investigation of defocusing and use of compressed breast phantom. *In: Fourth International Congress on the Ultrasonic Examination of Breast*. Jellins J., Kossoff G., Croll J., eds. Witton Press Pty. Ltd., Sydney, Australia.
- Kelly-Fry E., Morris S.T., Sanghvi N.T., and Madsen E.L. (1987) Frequency spectrum shifts of ultrasound echoes as a function of depth in a female breast. *Proc. of Jour. of Acoustical Society of America*, Supp 1, Vol. 81.
- Kelly-Fry E., Morris S.T., Jackson V.P., Holden R.W., and Sanghvi N.T. (1988) Variation of transducer frequency output and receiver band-pass characteristics for improved detection and image characterization of solid breast masses. (Paper in this publication).
- Kopans D.B., Meyer J.E. and Lindfors K.K. (1985) Whole breast US imaging: four-year followup. *Radiology* 157, 505-507.
- Madsen E.L., Zagzebski J.A., Banjavic, R.A. and Jutila, R.E. (1978) Tissue-mimicking materials for ultrasound phantoms. *Med. Phys.* 5, 391-394.
- Madsen E.L. (1980) Ultrasonically soft tissue mimicking material. *In Medical Physics of CT and Ultrasound: Tissue Imaging and Characterization* (Edited by G.D. Fullerton and J.A. Zagzebski, pp. 531-550.) American Institute of Physics, New York.
- Madsen E.L., Zagzebski J.A. and Frank G.R. (1982a) Oil-in-gelatin dispersions for use as ultrasonically tissue-mimicking materials. *Ultrasound Med. Biol.* 8, 277-287.
- Madsen E.L., Zagzebski J.A., Insana M., Burke T. and Frank G.R. (1982b) Ultrasonically tissue-mimicking liver including the frequency dependence of backscatter. *Med. Phys.* 9, 703-710.
- Madsen E.L., Insana M.F., Zagzebski J.A. and Frank G.R. (1984) Method of data reduction for accurate determination of acoustic backscatter coefficients. *J. Acoust. Soc. Am.* 76, 913-923.
- Sickles E.A., Filly R.A. and Callen P.W. (1983) Breast cancer detection with sonography and mammography: comparison using state-of-the-art equipment. *AJR* 140, 843-845.
- Sickles E.A. (1985) Breast imaging: a view from the present to the future. *Diag. Imag. Clin. Med.* 54, 118-125.
- Weber W., Sickles E., Callen P. and Filly R. (1985) Nonpalpable breast lesion localization: limited efficacy of sonography. *Radiology* 155, 783-784.
- Wu X.K., Goodsitt M.M. and Madsen E.L. (1988) Experimental test of a theoretical model for attenuation of longitudinal ultrasonic waves in materials simulating soft tissues. To be published in *J. Acoust. Soc. Am.*